PYROCLASTIC ERUPTIONS ON MERCURY: INSIGHTS INTO ERUPTION MECHANISMS FROM VENT MORPHOLOGY. L. M. Jozwiak[1], J. W. Head[1], and L. Wilson[2,1, 1]Dept. Earth, Environmental and Planetary Sciences, Brown University, Providence, RI 02912. [2]Lancaster Environment Centre, Lancaster University, Lancaster LA1 4YQ, UK (lauren_jozwiak@brown.edu)

Introduction: Prior to the MESSENGER (MErcury Surface, Space ENvironment, GEochemistry, and Ranging) mission to Mercury, there was active debate about the presence and extent of volcanic features [e.g. 1, 2, 3]. However, the first fly-by of the MESSENGER mission revealed substantial evidence for both smooth volcanic plains [4, 5], which had been postulated based on Mariner 10 data [1], and also evidence for explosive volcanic morphologies [4], which had not previously been observed.

The explosive volcanic features have been interpreted to be pyroclastic vents on the basis of their irregular and often elongated morphology, lack of associated raised crater rim, and the mantling morphology displayed by the surrounding pyroclastic deposit [6]. The pyroclastic deposit has diffuse boundaries, a high albedo when observed in MDIS (Mercury Dual Imaging System) [7] mono images, and a characteristic orange/red color ("red spot") when viewed in MDIS multispectral WAC analysis [8]. Kerber et al. [2011] [9] used MESSENGER flyby data to map 40 pyroclastic deposits, and Goudge et al. [2013] [10] mapped an additional 10 features using the first year of MESSENGER orbital data. Thomas et al. [2014] [11] used MESSENGER orbital data to map all "red spot" deposits across the surface of Mercury. We now present the first global morphologic analysis of vent morphology. We combine this analysis with morphometric analyses to assess possible eruption and formation mechanisms for mercurian pyroclastic vents.

Mercurian Vent Morphologies: Previous workers have used a combination of 1) physical vent morphology, 2) "red spot" color anomaly in MDIS multispectral mosaic images, and 3) high albedo deposit surrounding the vent morphology [6, 9, 10, 11] in the construction of their pyroclastic vent databases. We combined the previously constructed databases and analyzed all of the morphologies observed therein. In our classification, we sought to focus on those vents and deposits with a clearly volcanic origin and morphology. For this reason, we required all vent candidates to have a clearly-expressed physical vent morphology, and while we preferred the presence of a surrounding spectrally distinctive (most often "red spot") deposit, we did not require its presence. Using these criteria, our analysis produced a database of 100 pyroclastic vents of three main morphologic types (Fig. 1) 57 vents, 36 pits, and 7 vents-with-mounds.

The first morphologic type is the *vent* morphology (Fig. 1a), which is characterized by a long primary axis, a shorter secondary axis, and walls sloping to a narrow floor. In contrast, the *pit* morphology (Fig. 1b) characterizes vents with more equant axes and a flatter floor profile. The third morphology is named *vent-with-mound* (Fig. 1c), and is characterized by a vent circumscribing a central mound of material. These features have been previously described for both the irregular morphology observed in the Caloris basin [12], and also the nearly circular expressions observed outside the Caloris basin [13].

Vent Distribution and Morphometric Analysis: In order to assess the formation mechanism(s) of these vents, we performed a number of morphologic analyses. The distribution of vents compared with the distribution of Mercurian smooth plains [14] (Fig. 2) reveals no close spatial association of vents with smooth plains deposits; the only exception is the association of vents with the interior edge of the Caloris basin. This is in stark contrast to the Moon where both pyroclastic deposits [15] and floor-fractured craters (intrusive magmatic morphologies) [16] have a close spatial association with mare deposits. Additionally, volcanic morphologies (mare deposits and pyroclastic deposits) in lunar floor-fractured craters are located near the edges of the crater floor [16, 17], which is a consequence of the stress environment imparted by the subcrater magmatic sill. In contrast, mercurian pyroclastic vents are primarily located in the center of the crater floor and adjacent to crater central peaks.

We compared the average primary axis length for both vents and pits, and found an average primary axis length of 12.5 km for vents and 12.3 km for pits, with comparable standard deviations for the two morphologies. Both vent morphologies and pit morphologies are primarily located inside craters; 85% of vents and 84% of pits are located inside craters or basins. We use the crater degradation class [18] of the host crater as a proxy for vent formation time by placing an older bound on the vent age. The normalized data suggest that pits primarily form in craters of intermediate degradation class (3-4), whereas vents form primarily in craters with younger degradation classes (1-3). Combined with the previous analyses, this leads us to suggest that the separation between vents and pits is purely morphological and may represent the geometry of the intrusion and eruption. It is also possible that vent morphologies can degrade into pit morphologies through normal degradation and infilling processes.

We compared average primary axis length with crater degradation state. Mercury has experienced significant contraction over the past ~3.7 Ga [19], which would be predicted to inhibit volcanic activity [20], resulting in

fewer volcanic plains deposits and potentially smaller pyroclastic vents. However, an analysis of vent primary axis length as a function of crater degradation class reveals no such trend. The data are widely scattered indicating no correlation between host crater age and vent length. We similarly analyzed the relationship between vent primary axis length and radially averaged pyroclastic deposit length. The data are suggestive of some process for deposit removal via impact degradation and mixing, with most of the deposit radii being smaller than would be predicted for their vent size. Additionally, 19% of vents do not have a visible "red spot" pyroclastic deposit extending from the vent; this could be due to a gas-only venting as predicted for the Moon [21] and could also indicate some process(es) for deposit removal, such as regolith mixing.

Implications for Eruption Mechanisms: One interpretation of these features and deposits is that they represent caldera collapse into shallow magma reservoirs [22]. Our analysis of mercurian pyroclastic vent morphology, and the overall lack of evidence for shallow intrusions (such as the floor-fractured crater morphologies seen on the Moon [23]), suggest a different paradigm for intrusive magmatism and explosive volcanism on Mercury. Our data suggest that pyroclastic vents on Mercury are more readily explained by explosive venting of gas and foam in the tips of stalled dikes as seen locally on the Moon [24]. For example, in the southern part of the Orientale basin unassociated with mare material, a dark pyroclastic ring deposit 154 km in diameter is centered on an elongate 7.5 x 16 km depression interpreted to be the vent [24], and is an excellent lunar analog for the mercury pit craters and deposits [4]. In this context, the observed morphologic variation between vents and pits can be easily explained by differences in dike width or depth of stalling [4, 24]. In addition, normal morphologic degradation processes could transform a crisp vent morphology into a rounded pit morphology. The source and nature of the driving volatile/volatiles [6, 9, 10] is under investigation and we are currently exploring scenarios for volatile sources and evolution. Volatiles could be sourced from 1) the initial magma source, 2) formed via reactions within the magma (as with CO on the Moon [e.g. 25]), or 3) via magma/wall rock interactions [26], or some combination of these, as is the case on the Moon [21]. We can use the deposit radius to infer eruption velocity and volatile content [20], expanding the analysis of Kerber et al. [2009] [6]. Previous analyses of volatile gas fraction for mercurian eruptions suggest very high gas fractions, 5x the equivalent amount of CO on the Moon [6]. This could indicate convection of magma within the dike and a secondary enhancement in volatile abundance as a driver for eruptions, a process similar to that proposed for the Orientale dark mantle ring deposit on the Moon [24].

Conclusions: Pyroclastic vents on Mercury display three main morphologies: *vent*, *pit*, and *vent-with-mound*. A wide range of vent degradation states and ages suggests that pyroclastic vents are likely to have formed throughout the history of Mercury. The observed morphologies also suggest a formation mechanism different from magma reservoir formation and collapse [22] and different from the type of sill formation process observed in lunar floor-fractured craters [17]. We support the dike-degassing model [21, 23] to form the majority of mercurian vents, and we are currently investigating volatile evolution processes for this model.

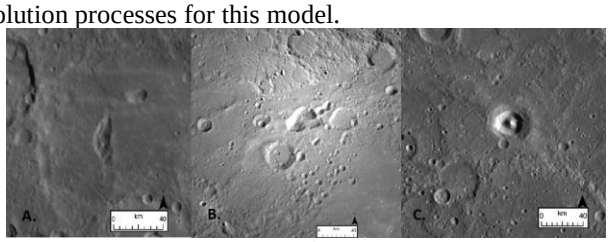

Figure 1: MDIS [5] mono images of mercurian pyroclastic vent morphologies: A) vent morphology, B) pit morphology, C) vent-with-mound morphology. A) Kipling crater (71.43° E, 19.21° S). B) NE Rachmaninoff vent (63.8° E, 35.8° N). C) (136.78° W, 3.54° S).

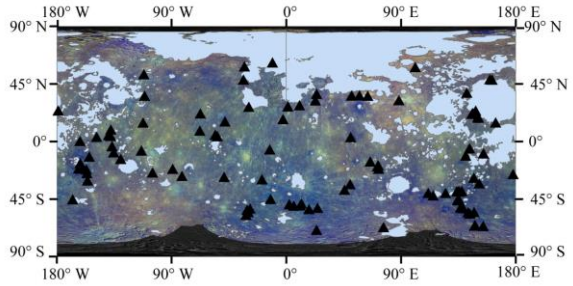

Figure 2: Global distribution of mercurian pyroclastic vents of clear volcanic origin, N = 100. With the exception of the Caloris basin, there is no clear spatial association of pyroclastic vents with smooth plains deposits [12]. MDIS 8-color base map (R: PC2, G: PC1, B: 430/560 nm) [6]. Smooth plains deposits shown in blue [12].

References: [1] Strom, R. G., et al. (1975) *JGR 80*, 2478-2507. [2] Wilhelms, D. E. (1976) *Icarus 28*, 551-558. [3] Head, J. W., et al. (2007) *Space Sci. Rev. 131*, 41-84. [4] Head, J. W., et al. (2009) *EPSL 285*, 227-242. [5] Head, J. W., et al. (2008) *Science 321*, 69-72. [6] Kerber, L., et al. (2009) *EPSL 285*, 263-271. [7] Hawkins III, S. E., et al. (2007) *Space Sci. Rev. 131*, 247-338. [8] Murchie, S. L., et al. (2008) *Science 321*, 73-76. [9] Kerber, L., et al. (2011) *PSS 59*, 1895-1909. [10] Goudge, T. A., et al. (2014) *JGR Planets 119*, 3, 635-658. [11] Thomas, R. J., et al. (2014) *JGR Planets 119*, 10, 2239-2254. [12] Rothery, D. A., Thomas, R. J., Kerber, L. (2014) *EPSL 385*, 59-67. [13] Thomas, R. J., et al. (2015) *PSS 108*, 108-116. [14] Denevi, B. W., et al. (2013) *JGR Planets 118*, 891-907. [15] Gaddis, L. R., et al. (2003) *Icarus 161*, 262-280. [16] Jozwiak, L. M., et al. (2012) *JGR Planets 117*, E11. [17] Jozwiak, L. M., Head, J. W., Wilson, L. (2015) *Icarus 248*, 424-447. [18] Prockter, L. M., et al. (2015) *AGU Fall Meeting 2015*, P53A-2016. [19] Byrne, P. K., et al. (2014) *Nature Geoscience 7*, 301-307. [20] Wilson, L., Head, J. W. (2003) *GRL 30*, 1605. [21] Wilson, L., Head, J. W. (2015) *Icarus*, Accepted. [22] Gillis-Davis, J. J., et al. (2009) *EPSL 285*, 243-250. [23] Head, J. W., et al. (2009) *EPSL 285*, 251-262. [24] Head, J. W., Wilson, L., Weitz, C. M. (2002) *JGR 107*, E1. [25] Rutherford, M. J., Papale, P. (2009) *Geology 37*, 3, 219-222. [26] Zolotov, M. Y. (2011) *Icarus 212*, 24-41.